Stick-sudden-rotation and structural polymorphism of (C70)mAun hybrid nanoclusters

Wang, Yitao; Kaya, Dogan; Gao, Jianzhi; Guo, Quanmin

DOI:
10.1021/acs.jpcc.9b01349

Stick-sudden-rotation and Structural Polymorphism of $(C_{70})_m$-$(Au)_n$ Hybrid Nanoclusters

Yitao Wang[1], Dogan Kaya[2], Jianzhi Gao[3], Quanmin Guo*[1]

[1]School of Physics and Astronomy, University of Birmingham, Birmingham B15 2TT, UK.

[2]Department of Electronics and Automation, Vocational School of Adana, Cukurova University, 01160 Cukurova, Adana, Turkey.

[3]School of Physics and Information Technology, Shaanxi Normal University, Xi'an 710119, China.

Abstract

We fabricated magic number $(C_{70})_m$-$(Au)_n$ clusters on the Au(111) substrate. These clusters are stable at room temperature, but display unpredictable rotational movement. The time duration between two successive rotations is in the order of ~hour. The cluster rotation is a thermally activated process due to energy fluctuation which is more significant for small clusters. We followed the rotational movement of $(C_{70})_{10}$-$(Au)_{35}$ clusters using scanning tunnelling microscopy. Our observation suggests that thermal fluctuation leads to rapid diffusion of Au atoms at the edges of the cluster and the cluster has many meta-stable configurations associated with structural polymorphism.

Keywords

Atomic cluster, diffusion, magic number cluster, edge diffusion, self-organization, nanostructures, gold, fullerene, C_{70}, scanning tunnelling microscopy.

Introduction

Atomic and molecular clusters are an important class of materials exhibiting size-dependent properties.[1-4] Great amount of effort has been devoted to the fine tailoring of the clusters including size-selection,[5,6] shape control[7] and surface passivation.[8] Metal clusters passivated with a molecular layer have demonstrated superior stability against sintering and degradation[9] and are thus potentially useful in aggressive environments such as electrolytes or biological systems.

Recently, we have succeeded in making magic number fullerene-metal hybrid clusters, $(C_{60})_m$-$(Au)_n$.[10] These clusters are self-assembled on the Au(111) substrate with the smallest cluster being $(C_{60})_7$-$(Au)_{19}$.[10] The clusters are stable up to 400 K as a result of effective interaction between the molecules and the Au atoms in the cluster. Here we investigate thermally induced cluster transformation with a view to understanding how the hybrid clusters diffuse, coalesce and ripen on the Au(111) surface.

Ostwald ripening and Smoluchowski ripening are the two dominant pathways for coarsening and growth.[11] As the most common ripening pathway, Ostwald ripening is characterised by shrinking of small sized clusters and growth of the large ones driven by the tendency to minimise the total free energy.[12-14] Smoluchowski ripening on the other hand, is featured by whole cluster displacement and merger of clusters as a result of cluster collision.[15] Both the two ripening pathways aim at reducing the system's total free energy with the help of mass transport.

For two-dimensional (2D) clusters supported on a substrate, the clusters tend to have a regular shape.[16] Adatoms on the surface of the substrate can act as the medium for mass

transport between different clusters.[17,18] Research about coarsening and positional change of 2D nanoclusters in homoepitaxial systems have been conducted on different metal surfaces such as Ag and Cu,[19-22] in which the same type of adlayer islands ripen in different pathways. For the $(C_{60})_m$-$(Au)_n$ cluster, the metal core consisting of *n* Au atoms is protected by the molecular "shell", and thus affecting both Ostwald and Smoluchowski ripening. In the work presented here, we have replaced C_{60} with C_{70} and created $(C_{70})_m$-$(Au)_n$ clusters. The overall property of the $(C_{70})_m$-$(Au)_n$ cluster is similar to that of $(C_{60})_m$-$(Au)_n$.

Experimental Methods

The experiments are performed using an Omicron variable temperature STM (VT-STM). The substrates are thin gold films grown on highly oriented pyrolytic graphite (HOPG) with physical vapour deposition. The Au films are about 200 nm thick and have a preferred orientation to expose the (111) planes. The Au films treated with cycles of Argon ion sputtering and thermal annealing to obtain clean and atomic smooth terraces. To grow $(C_{70})_m$-$(Au)_n$ magic number clusters, the Au/HOPG sample is firstly cooled down to 110 K, and ~0.15 ML gold atoms are deposited. This forms irregular Au islands at the elbow sites on the reconstructed gold substrate. We subsequently deposit ~0.05 ML of C_{70} molecules. The molecules become attached to the pre-existing Au islands. The sample is then slowly annealed to room temperature, leading to the formation of $(C_{70})_m$-$(Au)_n$ magic number clusters.

Results and discussion

The $(C_{70})_m$-$(Au)_n$ clusters are produced by sequential deposition of Au atoms and C_{70} molecules onto Au(111) at 110 K. Slow thermal annealing to room temperature (RT) resulted in self-assembled magic number clusters. Figure 1a shows an STM image acquired at RT.

Different-sized magic number clusters as well as compact C_{70} patches can be seen in the image. Figures 1b-d shows the three smallest clusters with the corresponding structural models displayed in Figures 1e-g. In a previous publication,[10] we reported the formation of $(C_{60})_m$-$(Au)_n$ clusters on Au(111) and found preferential nucleation of clusters at the elbow sites. In the present study, C_{60} molecules are replaced with C_{70}. We find that the general behaviour of $(C_{70})_m$-$(Au)_n$ clusters is very similar that of $(C_{60})_m$-$(Au)_n$. All clusters are confined by the discommensuration lines.[23,24] The nearest neighbour distance between C_{70} molecules is 1 nm which is the same as that for C_{60} inside the $(C_{60})_m$-$(Au)_n$ clusters. This suggests that the long axis of the C_{70} molecules is perpendicular to the Au(111) substrate. The structural models in Figs. 1e-h, following those developed for $(C_{60})_m$-$(Au)_n$ clusters,[10] are not derived from DFT calculations. They are constructed based on the experimentally measured molecule-molecule distances and by considering an appropriate distance between the C_{70} molecule and the step edges of the Au island. The $(C_{70})_m$-$(Au)_n$ clusters are stable at low temperatures. When scanned by the STM at 110 K, no changes to the clusters are observed. Thus, the STM tip alone is not able to induce movement of atoms/molecules in the cluster. We also use low tunnel currents of the order of 50 pA in order to minimise perturbation from the tip. At RT, the stability of the clusters shows some size dependence. Clusters containing more than six C_{70} molecules sitting on top of the gold islands are stable at RT showing no positional changes or rotation over many hours at least. The cluster shown in Fig. 1d has just three molecules sitting on the Au island. Smaller clusters are observed to rotate. The rotation has a stick-sudden-rotation pattern. A cluster can stay in one azimuthal orientation for many minutes or even up to an hour, and then it rotates suddenly into a different orientation.

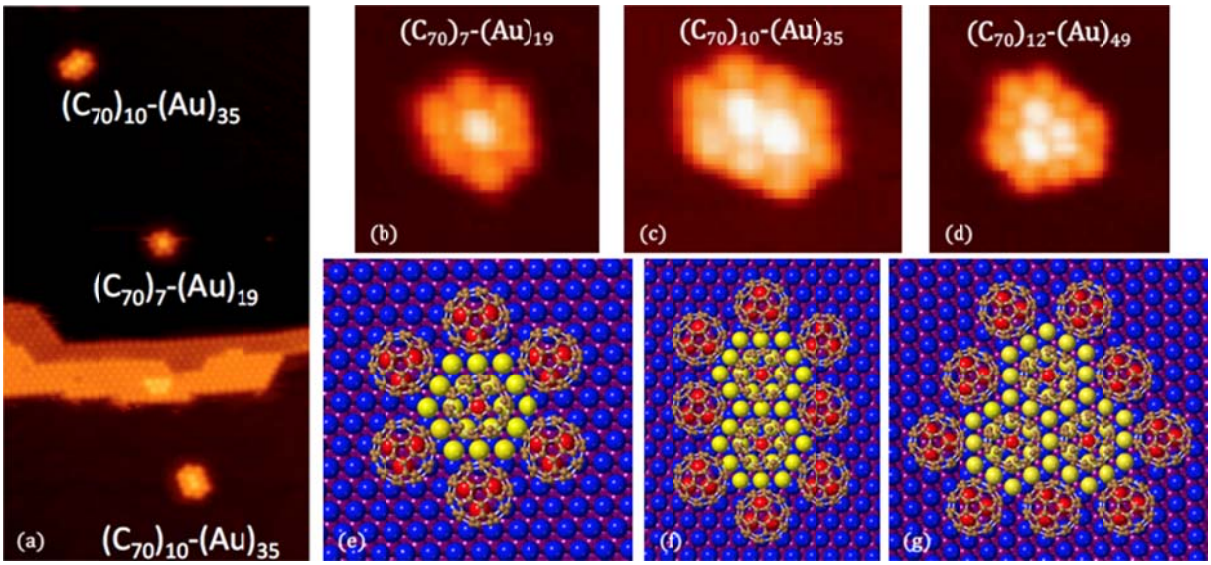

Fig. 1. (a) STM image showing the presence of different sized $(C_{70})_m$-$(Au)_n$ clusters, as well as close-packed C_{70} monolayer islands at steps. The detailed structures for $(C_{70})_7$-$(Au)_{19}$, $(C_{70})_{10}$-$(Au)_{35}$, and $(C_{70})_{12}$-$(Au)_{49}$, are shown in (b), (c) and (d), respectively. Structural models corresponding to the above three magic number clusters are displayed in (e), (f) and (g), respectively. Yellow spheres represent Au atoms within the cluster. Red spheres are Au atoms in direct contact with the C_{70} molecule.

The rotation of clusters is demonstrated by the STM images in Figure 2. Each image in Fig. 2 is shown with two different contrasts. The upper panel shows the cluster where the individual molecules are resolved. The lower panel shows contrast-enhanced image where the discommensuration lines of the reconstructed Au(111) surface can be seen. We have focused on the $(C_{70})_{10}$-$(Au)_{35}$ cluster because this cluster has a distinct shape so that its rotational movement can be easily identified. The $(C_{70})_7$-$(Au)_{19}$ cluster with its hexagonal shape, on the other hand, makes it harder to identify rotations if the rotation angle is 60 degrees. In Fig. 2a, there is a $(C_{70})_{10}$-$(Au)_{35}$ cluster alongside a $(C_{70})_{13}$-$(Au)_{51}$ cluster. As shown in Fig. 1f, the $(C_{70})_7$-$(Au)_{19}$ cluster has two edge sharing hexagons of gold atoms. The $(C_{70})_{13}$-$(Au)_{51}$ cluster

can be viewed as a natural extension of the $(C_{70})_7$-$(Au)_{19}$ cluster by having three edge sharing hexagons in a row. In all our experiments, the number of C_{70} molecules in a cluster can be accurately counted from the STM images, but the number of Au atoms within each cluster cannot be directly determined. The magic number for Au is inferred from the physical area occupied by the "bright" C_{70} molecules.

The $(C_{70})_{13}$-$(Au)_{51}$ cluster remains motionless over the many hours of observation. The $(C_{70})_{10}$-$(Au)_{35}$ cluster is found to "rotate" from time to time as evidenced by changes of the azimuthal orientation. Although it appears that the whole cluster has rotated, the apparent "rotation" is a consequence of the movement of individual atoms and molecules as will be discussed later. Here we use the $[11\bar{2}]$ direction as the reference and measure the angle, θ, between the long axis of the $(C_{70})_{10}$ cluster and the $[11\bar{2}]$ direction. Initially, the long axis of the $(C_{70})_{10}$-$(Au)_{35}$ cluster is parallel to the $[11\bar{2}]$ direction. This is assigned to the 0° state. In Figure 2a, the long axis of the $(C_{70})_{10}$ cluster is parallel to the $[11\bar{2}]$ direction, and hence $\theta = 0^o$. The cluster remains in this state for 15 minutes until it rotates suddenly by 5 degrees, Fig. 2b. After 15 minutes, the cluster is observed to have rotated again. In addition to the clear rotation of the cluster, there is also evidence that the centre of mass of the cluster has shifted slightly upon rotation. Most clusters are found at the elbow site. There are two types of elbows: the pinched elbow and the bulged elbow.[25] The cluster in Fig. 2 is located at a bulged elbow site while the cluster in Fig. 3 is at a pinched elbow site. A small fraction of clusters are found to have moved away from the elbow site, Fig. 4. The $(C_{70})_{10}$-$(Au)_{35}$ cluster in Fig. 4 is located at some distance away from the nearby elbow site. This cluster is observed to rotate as well.

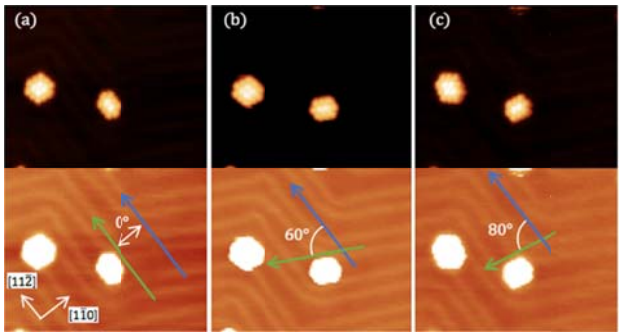

Fig. 2. STM images (30 nm x 30 nm) showing the rotation of a $(C_{70})_{10}$-$(Au)_{35}$ cluster at a bulged elbow site. Each image is shown with two different contrasts with the lower panel displaying clearly the discommensuration lines (DLs) of the herringbone reconstruction. The blue arrow indicates the [11$\bar{2}$] direction and the green arrow gives the direction of the long axis of the cluster. The angle is measured between the blue and green arrows. A positive value means that the cluster axis is rotated counter-clockwise from the [11$\bar{2}$] direction. Images are collected using -2.0 V sample bias voltage and 50 pA tunnel current.

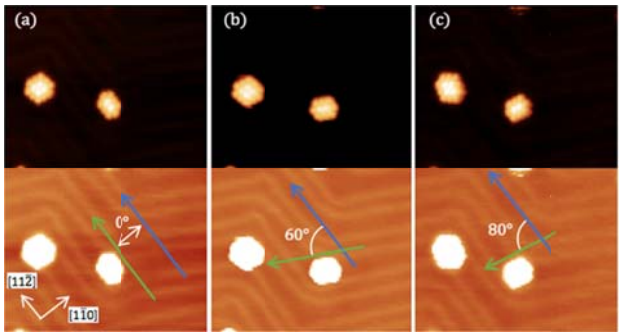

Fig. 3. STM images (30 nm x 30 nm) showing the rotation of a $(C_{70})_{10}$-$(Au)_{35}$ cluster at a pinched elbow site. Images are collected using -2.0 V sample bias voltage and 50 pA tunnel current.

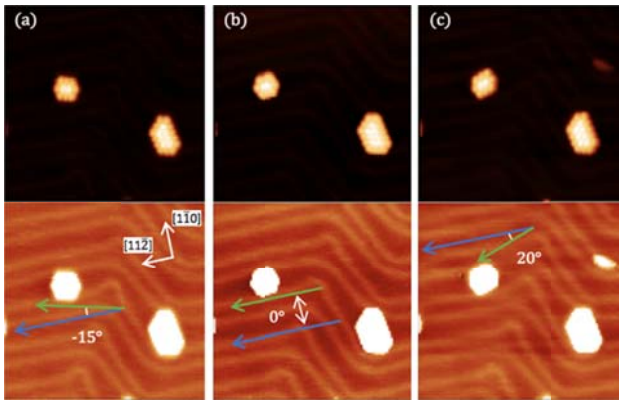

Fig. 4. STM images (30 nm x 30 nm) showing the rotation a $(C_{70})_{10}$-$(Au)_{35}$ cluster in the fcc region far away from any elbow sites. Images are collected using -2.0 V sample bias voltage and 50 pA tunnel current.

Figure 3 shows STM images where a $(C_{70})_{10}$ cluster at a pinched elbow site over a time duration of 3 hours. The cluster has undergone a rotation after 15 min., Fig. 3b, causing θ to change from 0 to 60 degrees. Due to the three-fold symmetry of the substrate, a rotational angle of 60 degrees brings the cluster back to effectively an identical azimuthal orientation as the starting configuration in Fig. 3a. However, there are many other rotational angles as already demonstrated by the images in Fig. 2. A rotational angle of 80 degrees is shown in Fig. 3c. Figure 4 shows a $(C_{70})_{10}$ cluster far away from any elbows. This cluster is confined by the two parallel discommensuration lines so that it has the freedom to move in between these two DLs, but it cannot cross either DLs to the neighboring hcp region. Here, this cluster is also seen to rotate. In Fig. 4a, θ is -15 degrees and in Fig. 4c, θ is 20 degrees.

Figure 5 gives more examples demonstrating the rotation of $(C_{70})_{10}$ clusters. The long axis of the cluster seems to be able to make a large number of angles to the $[11\bar{2}]$ direction. In order to quantify the appearance frequency of a particular azimuthal orientation of the cluster, we followed a particular cluster for ~96 h. The same cluster can be observed to take one

azimuthal orientation a number of times. Fig. 6 shows plots of the frequency of appearance for each θ as a function of θ. Fig. 6a, b, and c are plots for clusters at bulged elbow, pinched elbow, and non-elbow site, respectively. In each case, we find that θ can have quite a wide range of values. For instance, for the cluster at the bulged elbow site, θ ranges from -40° to 70°. The cluster has a preference of having $\theta = 0^o$ and $\theta = 60^o$, and this is consistent with the stability of the cluster in such a configuration.[10] The range of θ that the cluster can have seemed to depend on the physical dimensions of the fcc region which the cluster occupies. The width of the fcc region at the pinched elbow site is rather broad, and the corresponding θ ranges from -80° to 80° as seen in Fig. 6b. It seems that the discommensuration lines on either side of the cluster has some influence on the way it rotates. This is not surprising as the molecules tend to stay away from the DLs, because adsorption on top of the DLs is less stable.

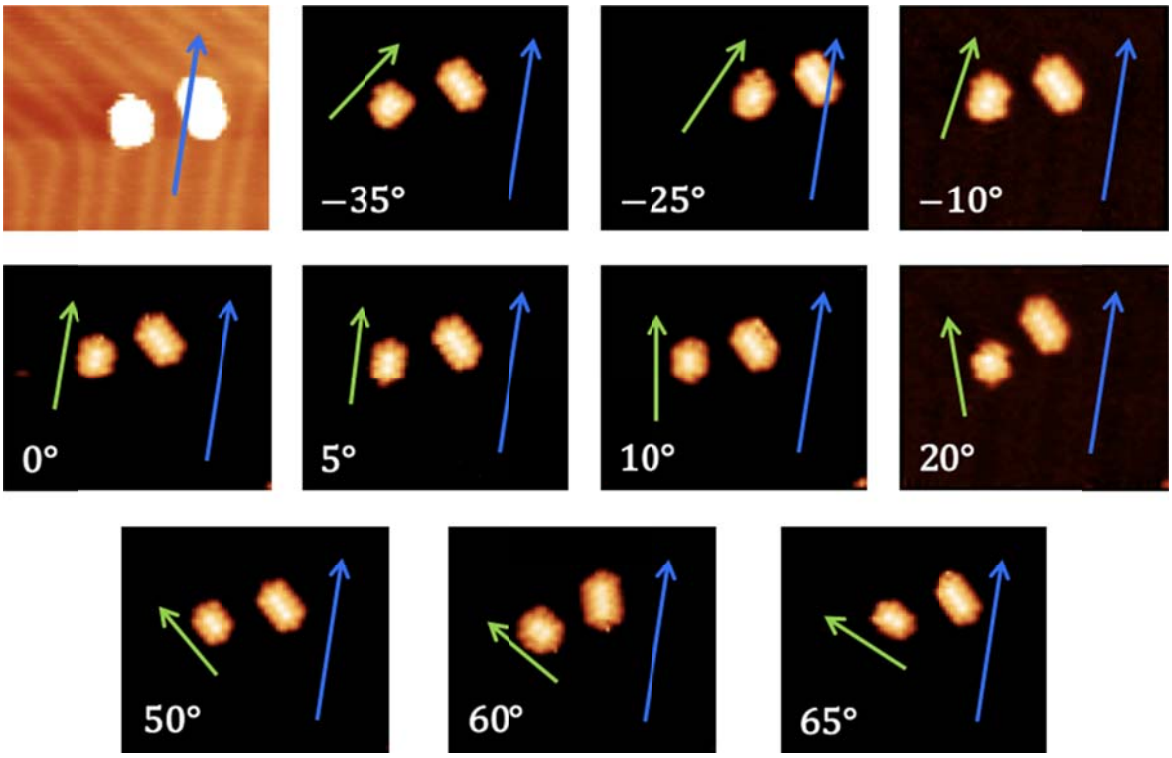

(a)

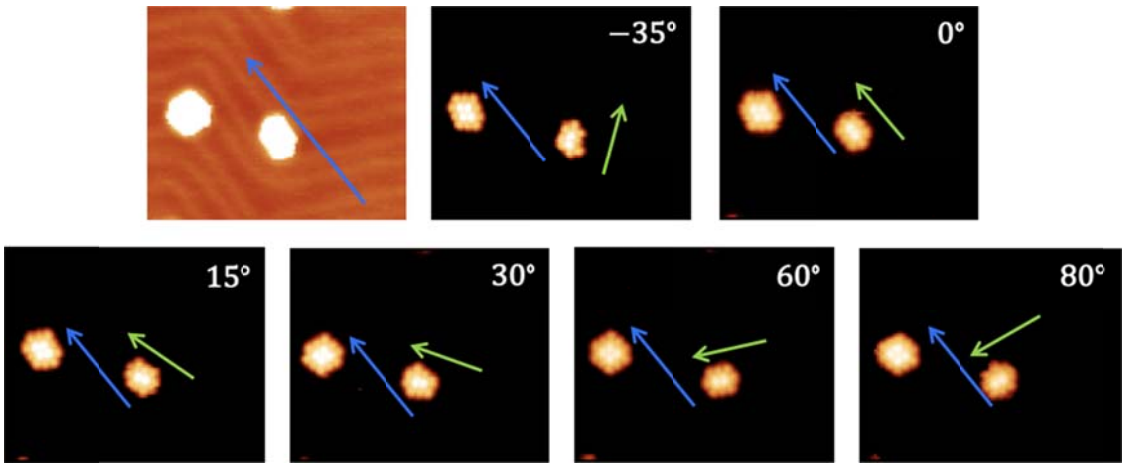

(b)

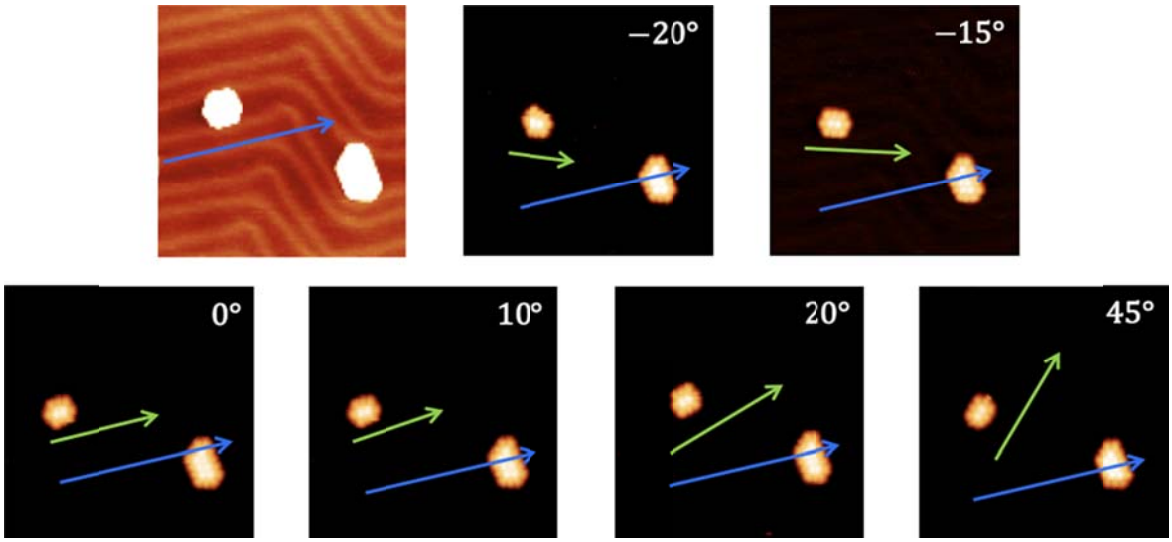

(c)

Fig. 5. STM images demonstrating various rotation angles for $(C_{70})_{10}$-Au_x clusters at bulged elbow (a); pinched elbow (b); and in fcc region at some distance away from neighbouring elbow sites (c).

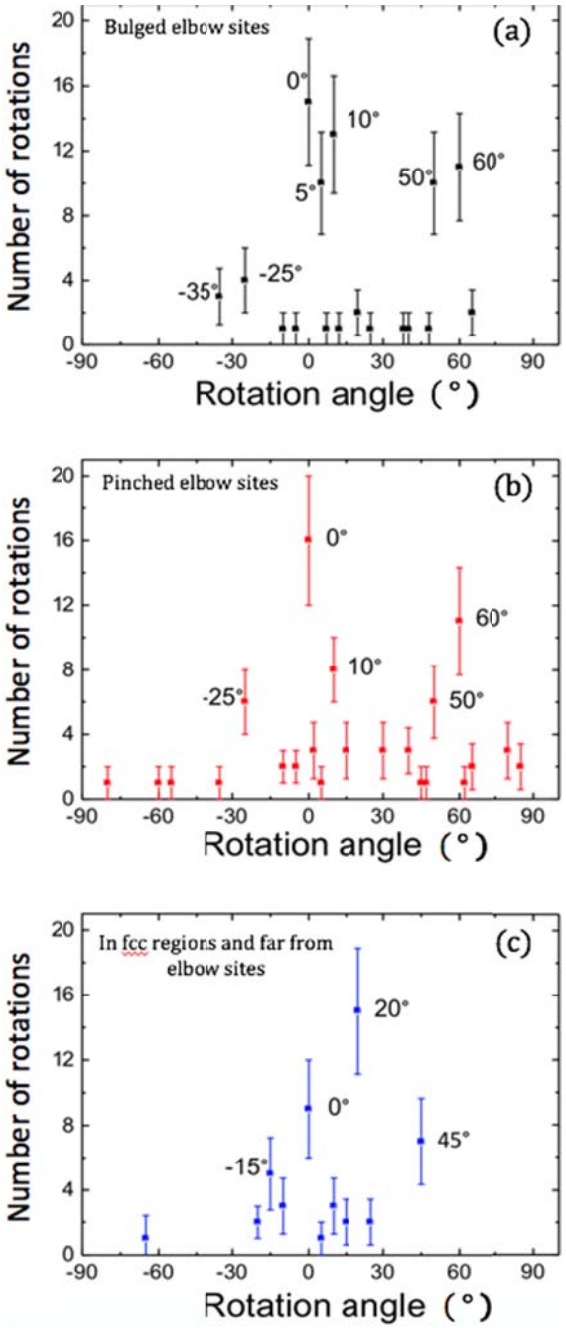

Fig. 6. Statistical analysis of the appearance frequencies of the various rotation angles. We simply counted the number of clusters with a particular angle for a given duration in time. A total number of 206 clusters have been taken into consideration.

What causes the cluster to rotate? Although the STM tip can disturb the clusters, the observed movement in this work is not due to tip effect. This can be verified by scanning two images

of the same area. After the first image is obtained, we wait for a while without scanning before the second image is acquired. We find that during the window of no active scanning, the cluster also rotates and the number of rotated clusters increases with the waiting time. Moreover, during normal scanning, we seldom observe cluster movement when the tip raster directly over the cluster. When scanned at 110 K, no cluster movement is observed. As the sample temperature increases, cluster rotation first appears when the sample temperature reaches around 250 K. All the above observations suggest that what we have seen is a thermally activated cluster movement. Each cluster can be treated as a small thermal system in contact with a reservoir (the Au substrate) at constant temperature. The internal energy of the cluster fluctuates. The fluctuation is relatively more significant for small clusters. This is why large clusters, with more than six molecules sitting on top of a Au island, are stationary at RT.

Due to thermal energy fluctuation, the Gibbs free energy of the cluster can reach a level such that the cluster becomes unstable. This leads to excessive movement of molecules and Au atoms resulting in re-organization. After each re-organization, the cluster moves into a different configuration and waits for the next move. What is interesting is that the cluster seems to have quite a large number of states. All these states may not have exactly the same free energy, but the energy difference between states is small. In order to explain the many different azimuthal orientations of the cluster, we propose a structural polymorphism for the cluster. Here structural polymorphism means that the Au cluster with a fixed number of atoms can have different geometric structures with more or less the same energy. Figure 7 gives a few structural models corresponding to different geometric structures of the Au island. Fig. 7a represents the perfect structure for a Au_{35} island that can make up the magic number $(C_{70})_{10}$-$(Au)_{35}$ cluster which fulfills the requirement that all edges of the Au island are

low step energy edges and all molecules maintain their preferred intermolecular distance for maximal van der walls interaction. A change in size and/or shape of the Au island directly affects the inter-molecular distance of C_{70}. Fig. 7b shows an Au island with 36 Au atoms. By putting two C_{70} molecules on top of this Au island and eight molecules around the edges, one can obtain a $(C_{70})_{10}$-$(Au)_{36}$ cluster with its long axis making a 10^o angle to the $[11\bar{2}]$ direction. Fig. 7c shows a gold island with 39 Au atoms which can be used to make a $(C_{70})_{10}$-$(Au)_{39}$ cluster. It is highly possible that the edges of the island contain defects. Obviously, these Au islands with different shapes have different energies. The ten C_{70} molecules, however, always retain a close-packed structure, no matter what the azimuthal orientation. Therefore, the close-packing of C_{70} molecules seems to be the dominant force that stabilizes the various shaped Au islands. The stability of magic number $(C_{60})_m$-$(Au)_n$ clusters has been well demonstrated by RT STM manipulation.[26] For$\theta = 0^o$the C_{70} molecules form a local $\left(2\sqrt{3} \times 2\sqrt{3}\right)$R30° structure, similar to what is found for the extended C_{70} and C_{60} monolayer on Au(111).[27] For other angles such as 10^o, 20^o etc, there are multiple adsorption sites for C_{70} molecules in the cluster and some adsorption sites may have a rather low symmetry. This does not present a significant problem because the C_{70} molecules do not form specific bonds with the gold substrate and the interaction is mainly of a charge transfer type.

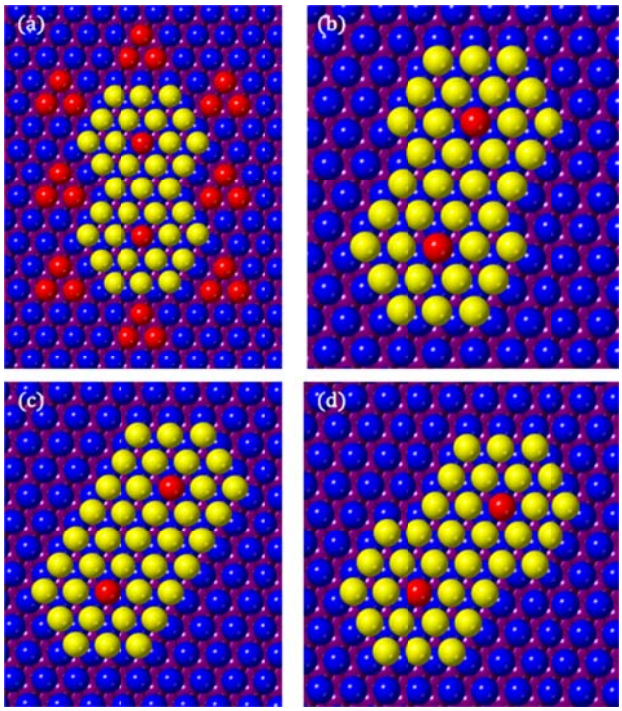

Fig. 7. Structural models proposed for single atomic layer Au islands consisting of ~35 Au atoms. (a) The ideal structure for the $(C_{60})_{10}$-$(Au)_{35}$ magic number cluster. (b) Au island with 36 Au atoms. The red spheres indicate where the two "bright" C_{70} molecules sit. (c) Au island with 39 Au atoms. (d) Au island with 36 Au atoms. When ten C_{70} molecules are added to the four different shaped Au islands, we can see the formation of clusters with their longer axis making 0^o, 10°, 30° and 50° angles to the $[11\bar{2}]$ direction, respectively.

Due to the stability of the magic number C_{70}-Au clusters, the conventional Ostwald ripening process is greatly modified. Evaporation of individual C_{70} molecules or Au atoms from a magic number cluster becomes difficult due to the interaction between of the molecular "shell" and the Au core. As we have already shown that a thermally disrupted cluster can quickly repair itself onsite. There are, however, cases where a cluster disintegrates after thermally agitated. In such cases, the C_{70} molecules and Au atoms released from the cluster diffuse independently and are later on captured by other neighboring clusters. There are a small number of large Au islands with island edges decorated by C_{70} molecules[28] giving rise

to the ring-like structure, Fig. 8. These large islands are effective atom and molecular sinks that capture individually diffusing atoms and molecules. Therefore, as temperature increases, ripening is characterized by the growth of a tiny fraction of the islands. Although $(C_{60})_m$-$(Au)_n$ and $(C_{70})_m$-$(Au)_n$ clusters behave very similarly on Au(111), the intermolecular interaction among C_{60} molecules is different from that among C_{70} molecules. This is partly due to the fact that the C_{70} molecules have a less spherical shape and thus the entropic contribution to molecular assembly is different.[29] It would be interesting to characterise the $(C_{60})_m$-$(Au)_n$ and $(C_{70})_m$-$(Au)_n$ clusters using spectroscopic techniques and determine the subtle differences between them. Moreover, the properties of a $(C_{60})_m$-$(Au)_n$ cluster are expected to be modified if one or more C_{60} molecule are substituted by C_{70}.

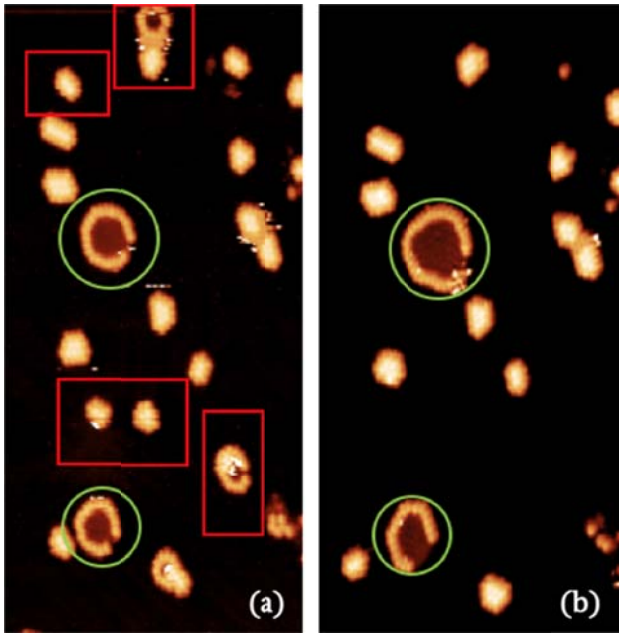

Fig. 8. Un-conventional ripening process. On the Au(111) surface, there are a small number of rather large Au islands such as the ones in green circles. Small compact clusters can disappear, with or without tip scanning at room temperature. The two images shown in (a) and (b) are taken 20 hours apart. The clusters highlighted with red boxes in (a) have disappeared during the 20 hours. The two large Au islands, in green

circles, have clearly grown in size and there are more C_{70} molecules decorating the step edges. This type of ripening favours the growth of very small number of large structures.

There are other factors that can alter the $(C_{70})_m$-Au_n clusters on Au(111). At RT, there are Au atoms diffusing on the surface. These atoms come from step edges. These free-diffusing atoms can be incorporated into a $(C_{70})_m$-Au_n cluster if they can pass through the C_{70} shell. Experimentally, it is difficult to investigate the effect of diffusing Au atoms because the STM cannot follow these atoms. However, the rotation shows clear size-dependent behavior with smaller clusters rotating more frequently. If changes of the clusters are due to capturing of surface Au atoms, one would expect the larger clusters to be affected more because of large collision cross-sections. An interesting experiment to clarify the role of surface Au atoms is to purposefully deposit Au atoms at RT and see if clusters change more frequently with higher concentration of surface Au atoms.

Conclusions

Fluctuation of thermal energy causes $(C_{70})_m$-Au_n clusters to occasionally quiver at room temperature. In most cases, the cluster does not disintegrate, but self-reorganizes by keeping its overall shape. The disturbed cluster usually changes its azimuthal orientation after thermal agitation. Many of the orientations are not aligned with major crystallographic directions on Au(111). It was proposed that the $(C_{70})_m$-Au_n cluster can exist in a large number of states with the Au core taking different structures, a phenomenon known as structural polymorphism. The polymorphism is favored for the C_{70}-Au system because of the lack of specific bonding between the C_{70} molecule and the Au substrate and that the bonding between Au and C_{70} from charge transfer is relatively weak.

References

[1] Palpant, B.; Prével, B.; Lermé, J.; Cottancin, E.; Pellarin, M.; Treilleux, M.; Perez, A.; Vialle, J. L.; Broyer, M. Optical properties of gold clusters in the size range 2-4 nm. *Phys. Rev. B.* **1998**, *57*, 1963.

[2] Pastor, G. M.; Dorantes-Dávila, J.; Bennemann, K. H. Size and structural dependence of the magnetic properties of small 3d-transition-metal clusters. *Phys. Rev. B.* **1989**, *40*, 7642.

[3] Muetterties, E. L. Molecular metal clusters. *Science* **1977**, *196*, 839.

[4] Wernsdorfer, W.; Sessoli, R. Quantum phase interference and parity effects in magnetic molecular clusters. *Science* **1999**, *284*, 133.

[5] Jarrold, M. F. Nano-surface chemistry on size-selected silicon clusters. *Science* **1991**, *252*, 1085.

[6] Buck, U.; Huisken, F. Infrared spectroscopy of size-selected water and methanol clusters. *Chem. Rev.* **2000**, *100*, 3863.

[7] Peng, X.; Manna, L.; Yang, W.; Wickham, J.; Scher, E.; Kadavanich, A.; Alivisatos, A. P. Shape control of CdSe nanocrystals. *Nature* **2000**, *404*, 59.

[8] Huang, X.; Lindgren, E.; Chelikowsky, J. R. Surface passivation method for semiconductor nanostructures. *Phys. Rev. B.* **2005**, *71*, 165328.

[9] Brust, M.; Walker, M.; Bethell, D.; Schiffrin, D. J.; Whyman, R. Synthesis of thiol-derivatised gold nanoparticles in a two-phase liquid–liquid system. *J. Chem. Soc. Chem. Commun.* **1994**, *7*, 801.

[10] Xie. Y. C.; Lin. T.; Guo, Q. Cooperative assembly of magic number C_{60}-Au complexes. *Phys. Rev. Lett.* **2013**, *111*, 186101.

[11] Zinke-Allmang, M.; Feldman, L. C.; Grabow, M. H. Clustering on surfaces. *Surf. Sci. Rep.* **1992**, *16*, 377.

[12] Thiel, P. A.; Shen, M.; Liu, D. J.; Evans J. W. Coarsening of two-dimensional nanoclusters on metal surfaces. *J. Phys. Chem. C.* **2009**, *113*, 5047.

[13] Morgenstern, K.; Rosenfeld, G.; Comsa, G. Local correlation during Ostwald ripening of two-dimensional islands on Ag (111). *Surf. Sci.* **1999**, *441*, 289.

[14] Icking-Konert, G. S.; Giesen, M.; Ibach, H. Decay of Cu adatom islands on Cu (111). *Surf. Sci*. **1998**, *398*, 37.

[15] Von Smoluchowski, M. Drei vortrage uber diffusion. Brownsche bewegung und koagulation von kolloidteilchen. *Phys. Z.* **1916**, *17*, 585.

[16] Röder, H.; Hahn, E.; Brune, H.; Bucher, J. P.; Kern, K. Building one-and two-dimensional nanostructures by diffusion-controlled aggregation at surfaces. *Nature* **1993**, *366*, 141.

[17] Ala-Nissila, T.; Ferrando, R.; Ying, S. C. Collective and single particle diffusion on surfaces. *Adv. Phys.* **2002**, *51*, 949.

[18] Bulou, H.; Bucher, J. P. Long range substrate mediated mass transport on metal surfaces induced by adatom clusters. *Phys. Rev. Lett.* **2006**, *96*, 076102.

[19] Wen, J. M.; Evans, J. W.; Bartelt, M. C.; Burnett, J. W.; Thiel, P. A. Coarsening mechanisms in a metal film: from cluster diffusion to vacancy ripening. *Phys. Rev. Lett.* **1996**, *76*, 652.

[20] Layson, A. R.; Evans, J. W.; Fournée, V.; Thiel, P. A. The effect of common gases on nucleation of metal islands: The role of oxygen in Ag (100) homoepitaxy. *J. Chem. Phys.* **2003**, *118*, 6467.

[21] Hannon, J. B.; Klünker, C.; Giesen, M.; Ibach, H.; Bartelt, N. C.; Hamilton, J. C. Surface self-diffusion by vacancy motion: Island ripening on Cu(001). *Phys. Rev. Lett.* **1997**, *79*, 2506.

[22] Rokni-Fard, M.; Guo, Q. Biased Ostwald ripening in site-selective growth of two-dimensional gold clusters. *J. Phys. Chem. C.* **2018**, *122*, 7801.

[23] Barth, J. V.; Brune, H.; Ertl, G.; Behm, R. Scanning tunneling microscopy observations on the reconstructed Au (111) surface: Atomic structure, long-range superstructure, rotational domains, and surface defects. *Phys. Rev. B.* **1990**, *42*, 9307.

[24] Huang, K. G.; Gibbs, D.; Zehner, D. M.; Sandy, A. R.; Mochrie, S. G. J. Phase behavior of the Au (111) surface: Discommensurations and kinks. *Phys. Rev. Lett.* **1990**, *65*, 3313.

[25] Chambliss, D. D.; Wilson, R. J.; Chiang, S. Nucleation of ordered Ni island arrays on Au (111) by surface-lattice dislocations. *Phys. Rev. Lett.* **1991**, *66*, 1721.

[26] Kaya, D.; Bao, D-L.; Palmer, R. E.; Du, S-X.; Guo, Q. Tip-triggered thermal cascade manipulation of magic number gold–fullerene clusters in the scanning tunnelling microscope. *Nano Lett.* **2017**, *17*, 6171.

[27] Altman, E. I.; Colton, R. J. Nucleation, growth, and structure of fullerene films on Au (111). *Surf. Sci.* **1992**, *279*, 49.

[28] Xie, Y-C.; Rokni-Fard, M.; Kaya, D.; Bao, D-L.; Palmer, R. E.; Du, S-X.; Guo, Q. Site-specific assembly of fullerene nanorings guided by two-dimensional gold clusters. *J. Phys. Chem. C.* **2016**, *120*, 10975.

[29] Guo, L.; Wang, Y-T.; Kaya, D.; Palmer, R. E.; Chen, G-D.; Guo, Q. Orientational epitaxy of van der Waals molecular heterostructures. *Nano Lett.* **2018**, *18*, 5257.

TOC graphic

$(C_{70})_{10}$-$(Au)_{35}$ magic number cluster